Lab on a Chip

PAPER

View Article Online
View Journal | View Issue

Cite this: *Lab Chip*, 2026, **26**, 2565

Digitally programmable microfluidic valving for autonomous, high-resolution continuous chromatographic purification

Yi-Cheng Liao,†[a] Chih-Yi Huang,†[ab] Yu-Chuan Tang,†[a] Cheng-Hsian Wu,[a] Yu-Hsuan Chi,[a] I-Wei Chen,[a] Hsuan-Yu Mu,[ac] Ya-Hui Lin,[a] Yunching Chen,[c] Fu-Fei Hsu[d] and Jen-Huang Huang *[a]

Continuous microscale purification requires analytical methods that provide deterministic fluid handling, precise temporal control, and contamination-free fraction discrimination. Existing microfluidic and benchtop chromatography systems only partially address these needs, leaving a gap for methods that support tightly coordinated, programmable purification cycles. This work presents a microfluidic continuous protein purification method that uses digitally programmable inlet (ICV) and collection (CCV) valves to establish a logic-driven chromatography operation. Sub-second buffer switching and deterministic routing across parallel affinity columns enable a reproducible and algorithm-defined purification sequence. Temporal gating through the CCV provides real-time, profile-guided fraction selection that isolates high-concentration eluates while effectively removing tailing segments. Using GFP-His_6 as a model substrate, the system maintains 70–89% purity over ten uninterrupted cycles, demonstrating strong cycle-to-cycle stability. Purification of His_6-tagged TRAIL further confirms compatibility with structurally sensitive biologics and preservation of functional activity. The compact, modular, and single-use architecture minimizes dead volume, prevents cross-contamination, and accommodates diverse chromatographic modes. By combining programmable valve logic with time-resolved elution control, this work advances microfluidic platforms from diagnostic tools toward autonomous and precision-controlled process operations. The method provides a broadly applicable analytical framework for microscale purification and supports the development of next-generation bioseparation and continuous biomanufacturing technologies.

Received 7th January 2026,
Accepted 19th March 2026

DOI: 10.1039/d6lc00015k

rsc.li/loc

Introduction

Biopharmaceuticals, including monoclonal antibodies, recombinant proteins, and therapeutic enzymes, have become central to modern therapeutics due to their molecular specificity and improved safety profiles.[1–4] However, despite extensive progress in upstream cell engineering and expression technologies, downstream purification remains one of the most resource-intensive and rate-limiting components of biomanufacturing.[5] Conventional precipitation-based purification commonly fails to achieve the resolution required for therapeutic-grade biomolecules,[6–8] while affinity chromatography, though dominant in industry, still relies on manual buffer switching, batch-wise operation, and operator-dependent timing, all of which restrict throughput and compromise reproducibility.[9–11]

As biomanufacturing accelerates toward intensified and continuous processing paradigms, purification systems are increasingly expected to sustain uninterrupted operation, transition dynamically between chromatographic phases, and coordinate multiple columns with precise temporal control.[12,13] These requirements have accelerated interest in continuous downstream strategies, which offer improved productivity, robustness, and resource efficiency but demand purification methods capable of rapid, programmable buffer routing and automated definition of eluate boundaries.[14] In parallel, single-use technologies (SUT) have transformed bioprocessing practice by reducing cleaning and validation burdens, minimizing cross-contamination, and enabling modular or small-batch manufacturing.[15] These trends collectively highlight a growing need for purification platforms that combine real-time fluidic control, contamination-free operation, and disposable modules capabilities that conventional chromatography systems and

[a] *Department of Chemical Engineering, National Tsing Hua University, Hsinchu 300044, Taiwan. E-mail: jenhuang@mx.nthu.edu.tw*
[b] *Department of Biomedical Engineering and Environmental Sciences, National Tsing Hua University, Hsinchu 300044, Taiwan*
[c] *Institute of Biomedical Engineering, National Tsing Hua University, Hsinchu 300044, Taiwan*
[d] *Institute of Cellular and Organismic Biology, Academia Sinica, Taipei 115201, Taiwan*
† These authors contributed equally.

existing automated platforms rarely combine within a unified framework.

Microfluidics provides a compelling foundation for such integration. Its low reagent consumption, rapid mass transfer kinetics, and fine temporal control made microscale systems increasingly attractive for developing next-generation purification methodologies.[16,17] However, most reported microfluidic purification devices employ static channel designs, single-column formats, or limited actuation schemes that lack the programmable logic required for synchronized multi-column operation or real-time discrimination of eluate composition.[18,19] As a result, these devices demonstrate the feasibility of microscale chromatography but do not yet constitute scalable methodological frameworks suited for continuous biomanufacturing. The field therefore requires method-level innovations that embed routing logic, phase recognition, and coordinated actuation into a coherent and disposable purification strategy.

This work establishes a microfluidic continuous protein purification (MCPP) strategy that reframes chromatography as a programmable, logic-driven operation rather than a device-level fluid routing task. The platform integrates two digitally programmable valve modules: an inlet control valve (ICV) for sub-second buffer reconfiguration and a collection control valve (CCV) for temporally gated fraction selection, formalizing chromatographic decision-making into deterministic fluidic logic. In contrast to existing microfluidic valves, rotary valves, or automated chromatography modules that primarily automate flow routing, the ICV–CCV architecture embeds purification rules directly into valve state transitions, enabling autonomous coordination of buffer delivery, column cycling, and fraction discrimination. This method-level integration supports synchronized multi-column workflows, real-time boundary recognition, and contamination-minimized recovery within a compact, modular, and fully disposable format. The generality of the framework is demonstrated using His_6-tagged model and therapeutic proteins, spanning both robust reporters and structurally sensitive biologics. Collectively, the MCPP platform defines a generalizable analytical methodology for microscale purification, positioning programmable microfluidic systems as autonomous and precision-controlled process tools aligned with emerging demands in continuous, intensified, and single-use biomanufacturing.

Materials and methods

Device design and fabrication

The microfluidic valve device was fabricated using a multilayer polymer manufacturing approach.[20] Device geometries were designed in 2D using Solid Edge (ST9, Siemens PLM Software, USA). PET (0.25 mm, Formosa Idemitsu Petrochemical Corporation, Taiwan) and acrylic layers (1.5 mm, Formosa Idemitsu Petrochemical Corporation, Taiwan) were cut with a CO_2 laser cutter (PLS6.75, Universal Laser System, USA) equipped with 10.6 μm (10–75 W) or 9.3 μm (30–70 W) lasers, using either inert gas or air assist to improve cut quality. PC layers (3 mm, Formosa Idemitsu Petrochemical Corporation, Taiwan) were machined using a 4-axis milling machine (Modela MDX-40A, Roland DG, Japan) at 4500–15 000 rpm. Cut layers were cleaned with ethanol to remove debris and assembled using pressure-sensitive silicone adhesive tape (9122, 3M, USA), applying uniform pressure with a roller to ensure complete bonding and eliminate air gaps. Nitrile butadiene rubber (NBR) O-rings (Cheng Feng Rubber, Taiwan) with an inner diameter of 1 mm, outer diameter of 3 mm, and cross-section width of 1 mm were used to seal channel junctions during the assembly to achieve a fully sealed microfluidic valve structure.

System setup

We developed a fully automated platform for continuous protein purification. At the front end, four reservoirs contained the sample, wash, elution, and re-equilibration buffers. These buffers were formulated for isocratic elution in affinity chromatography, with flexibility to modify compositions according to purification requirements. Each buffer was delivered by an individual peristaltic pump, assembled by mounting a 4-roller pump head (Runze Fluid, China) onto a stepper motor (NEMA 17, DMX-K-SA-17, Arcus Technology, USA). Pump operation was computer-controlled, enabling pre-programmed scheduling of buffer identity, flow rate, and timing. Pump and valve actuation were executed using a custom PC-based graphical user interface (GUI) developed by an external engineering vendor, which imports a CSV-based operation table defining step-wise buffer selection, run time, and motor speed/rotation parameters. Buffers were routed into the ICV, also actuated by an identical stepper motor, with valve positions determined by motor rotation angles to direct flow toward designated purification columns. Automated switching between buffers ensured uninterrupted operation. Purification columns were housed in a refrigerated compartment maintained at 4 °C to preserve protein integrity. Eluates were directed to the CCV, driven by the same stepper motor model, which was programmed to isolate fractions within the optimal elution window based on real-time profiling. The control software synchronized valve actuation and pump operation, allowing fully coordinated switching and fraction collection without manual intervention. Both the motor driver electronics and the hardware–software interface were custom-built by a local manufacture (ROBUST Technology, Taiwan).

Material preparation

Imidazole-based buffers (pH 7.4) were prepared for His-tag affinity purification. Wash buffer contained 20 mM imidazole (A10221.22, ThermoFisher, USA), 500 mM NaCl (S9888, Sigma-Aldrich, USA), and 20 mM Tris (GE17-1321-01, Sigma-Aldrich, USA). Elution buffer contained 250 mM imidazole, 500 mM NaCl, and 20 mM Tris. Re-equilibration buffer consisted of PBS.

Two types of columns were used for protein purification: pre-packed HisTrap HP 1 mL columns (17524801, Cytiva, Sweden) and custom gravity-flow polypropylene columns packed with Ni-NTA agarose (30210, QIAGEN, Germany). Custom

columns were fitted with lid adaptors to connect 1/16″ silicone tubing (ABW00002, TYGON, France) for leak-free integration. Resin loading, PBS rinsing, and storage at 4 °C were performed to maintain resin hydration and readiness for use.

E. coli GFP-His_6 lysate, RFP lysate (AssemZyme, Taiwan), and His-tagged human TRAIL lysate were used for platform validation. Human TRAIL was expressed from pQE-hTR (Addgene, plasmid no. 21811) transformed into *E. coli* BL21 (DE3). Transformation, protein induction (0.5 mM IPTG, 30 °C, 3 h), cell harvesting, and lysis (sonication in β-ME/PMSF buffer with NP-40) followed standard protocols. Lysates were clarified by centrifugation (36 000 rpm, 20 min, 4 °C), filtered (0.22 μm), and diluted with PBS prior to loading.

Protein analysis

Protein concentration was determined using the Pierce™ Coomassie Plus (Bradford) assay kit (Thermo Fisher Scientific, USA) with bovine serum albumin (BSA) as the calibration standard. Absorbance was measured at 595 nm, and protein concentrations were calculated from the standard calibration curve. Protein purity was subsequently evaluated based on SDS-polyacrylamide gel electrophoresis (SDS-PAGE). Protein bands resolved by SDS-PAGE and visualized by Coomassie Brilliant Blue staining were used as the basis for quantitative purity analysis. Band intensities were quantified using ImageQuant™ TL 8.1 analysis software (Cytiva, USA) after background subtraction to remove noise and non-specific signals. The purity of the target protein was calculated as the ratio of the integrated intensity of the target protein band to the total intensity of all detectable protein bands in the same lane, expressed as a percentage according to eqn (1).

$$\text{Purity}\,(\%) = \frac{\text{Target protein area}}{\text{Total peaks area}} \times 100\% \quad (1)$$

Cell culture

A549 human lung carcinoma cells (RRID:CVCL_0023) were obtained from the Bioresource Collection and Research Centre (BCRC 60074, Hsinchu, Taiwan). Cells were maintained in high-glucose DMEM (SH30022.01, HyClone, GE Healthcare Life Sciences, USA) supplemented with 10% fetal bovine serum (FBS; SH30084.03, HyClone, GE Healthcare Life Sciences, USA) and 1% penicillin/streptomycin (SV30010, HyClone, GE Healthcare Life Sciences, USA) at 37 °C in a humidified atmosphere containing 5% CO_2. All cell lines were authenticated by the supplier and routinely tested for mycoplasma contamination using PCR-based assays. No contamination was detected during the study.

Cell viability assay

Following 24 h hTRAIL exposure, cells embedded in matrix gel were incubated with 40 μM calcein AM (L3224, Thermo Fisher Scientific, USA) for 15 min in the dark in the 37 °C incubator. Fluorescence imaging was performed using an iRiS™ Digital Cell Imaging System (Logos Biosystems, Korea) and observe to determine the positive signals of ethidium homodimer-1 (ex/em = 490/610) and calcein AM (ex/em = 490/520). Cell viability was normalized to untreated controls.

Statistics and reproducibility

Statistical analyses were performed using the GraphPad Prism 9 software (GraphPad, USA). One-way analysis ANOVA was used to compare the differences between single groups. Data are presented graphically as mean ± SD. The values were normally distributed. *P*-Values of less than 0.05, 0.01, and 0.001 were considered statistically significant for one, two, and three stars, respectively.

Results

System overview

Affinity chromatography is a cornerstone in downstream bioprocessing due to its ability to exploit the specific and reversible interactions between target proteins and immobilized ligands. However, conventional batch-based workflows are constrained by discrete operation steps—sample loading, washing, elution, and re-equilibration—that require manual intervention or complex automation, resulting in increased downtime, inconsistent yield, and poor scalability. To overcome these limitations, we engineered a fully integrated, continuous-flow protein purification platform with digitally programmable microfluidic control (Fig. 1 and S1A and B). The system is built around a compact architecture and leverages rotational microvalve mechanisms to precisely synchronize reagent delivery and product collection in real time. This design enables autonomous operation without manual switching or flow interruption, thus supporting uninterrupted purification cycles with minimal human oversight.

The platform consists of five primary modules: (i) four buffer reservoirs corresponding to sample (S), wash (W), elution (E), and re-equilibration (R), positioned externally to supply reagents to the system; (ii) four individually addressable peristaltic pumps mounted on the platform for precise and independent buffer delivery; (iii) a programmable ICV that functions as the fluidic entry interface of the platform, receiving pump-driven buffers and directing selected streams into designated flow paths; (iv) four parallel affinity chromatography columns were maintained at a controlled temperature controller to ensure optimal binding kinetics; and (v) a CCV responsible to collect the target fractions from the columns for dynamic product fractionation (Fig. 1A). Each peristaltic pump consists of a stepper motor coupled to a six-roller pump head; thus, modulation of flow rate is achieved through direct motor control. Similarly, both ICV and CCV are actuated by stepper motors. To ensure coordinated actuation across modules, all motors are centrally controlled *via* the control software, enabling synchronized operation, programmable sequencing, and precise temporal regulation of fluid handling steps. The

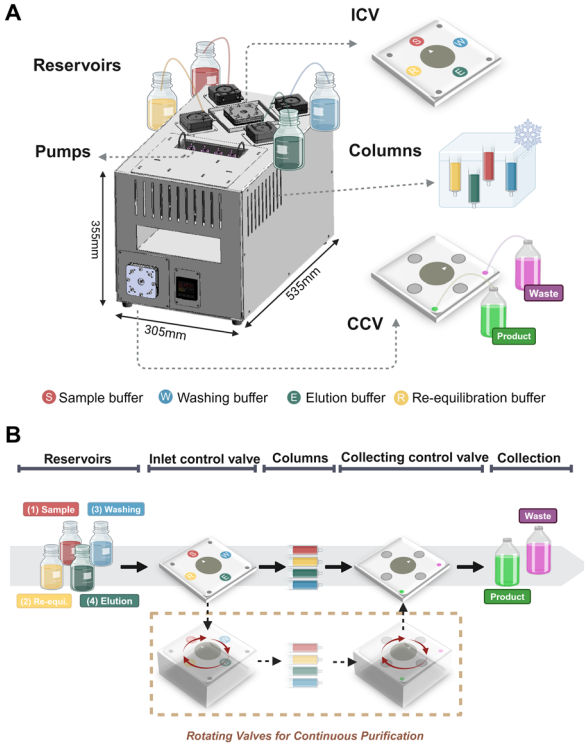

Fig. 1 Programmable MCPP platform. (A) MCPP platform comprising five key modules: four buffer reservoirs (sample, wash, elution, and re-equilibration), four independently operated peristaltic pumps, an ICV, four parallel affinity chromatography columns housed in a temperature-controlled chamber, and a CCV. The system integrates programmable, rotation-based flow switching with parallel affinity purification in a compact footprint (305 × 535 × 355 mm). (B) Schematic workflow of the purification cycle. Buffers are pumped into the ICV, which sequentially directs flow to individual columns based on programmed timing. Eluates are transferred to the CCV, which selectively collects high-concentration fractions and discards low-concentration waste, enabling real-time, continuous fractionation. Created with BioRender.

programmed sequences are executed through a PC-based GUI that imports a CSV-defined operation table (step sequence), where each step specifies the intended pump/valve state (*e.g.*, switch position/output position), motor speed/rotation parameters, and run time (Fig. S1C).

The ICV is a rotating disc that directs input buffers to designated columns based on a user-defined temporal sequence, allowing synchronized columns cycling across multiple purification stages. After each chromatographic step, effluents flow into the CCV, which performs real-time assessment of elution profiles and selectively channels high-concentration fractions to the product reservoir while diverting dilute fractions to waste. The CCV's programmable actuation allows for precise time-gated collection, enhancing product purity without the need for gradient elution or offline analysis (Fig. 1B).

To clarify the system-level integration (dashed box in Fig. 1B), the pumps, ICV, column module, and CCV are integrated within a single enclosure that contains the mechanical mounts, tubing manifolds, and centralized control electronics. The buffer reservoirs remain external and are connected to the enclosure *via* tubing, whereas the four affinity columns are housed in an internal temperature-controlled compartment to maintain low-temperature operation during continuous cycling. All stepper motors (four pumps, ICV, and CCV) are connected to a common motor-driver module and operated under a unified control sequence that specifies motor speed (flow rate), valve angle (routing state), and timing (stage duration), thereby enabling deterministic multi-column operation and synchronized fraction collection. The GUI executes this sequence by importing a CSV operation table and transmitting the corresponding motor-control commands from the PC to the motor driver/controller, ensuring repeatable actuation of predefined pump speeds and valve positions across runs.

By integrating these components into a modular and programmable platform, the system supports fully continuous purification with temporal resolution, high flexibility, and minimal dead volume. This architecture lays the foundation for intelligent biomanufacturing workflows capable of adapting to diverse protein targets and upstream production conditions.

Working principle

The core technology of this continuous purification system is a pair of custom-engineered programmable microfluidic valves: the ICV and the CCV which together orchestrate spatiotemporal routing of fluids with high precision and automation. Both valves share a multilayered architecture comprising four functional layers: the top layer, flow distribution layer, rotational valve layer, and bottom routing layer (Fig. 2). This modular design supports independent control over input delivery (ICV) and output selection (CCV), enabling synchronized, contamination-free operation. In the ICV, fluid from four buffer reservoirs, including sample, wash, elution, and re-equilibration, is delivered through inlet lines connected to the top layer. These lines feed into the flow distribution layer, which is composed of two stacked microfluidic layers arranged in a radially interleaved pattern (Fig. S2A and B). This design ensures even distribution of fluids from the center outward while minimizing backpressure and interchannel interference. The flow layer is partitioned into four quadrants, each connected to a dedicated purification column (C1–C4), allowing for independent routing of reagents during each purification stage.

Centrally positioned beneath the flow layer is the valve layer, which houses a stepper motor to drive rotational disc embedded with 16 circumferential through-holes. These ports act as programmable fluidic gates: (1) when aligned with both upstream (flow layer) and downstream (bottom layer) channels, fluid passes through vertically; (2) when misaligned, the pathway is blocked. This binary gating logic enables precise, on-demand channel switching without the need for external actuators. Leak-free operation is maintained through elastomeric O-rings seated in precision-milled grooves around each port, which deform during compression to create pressure-tight, reversible seals throughout valve

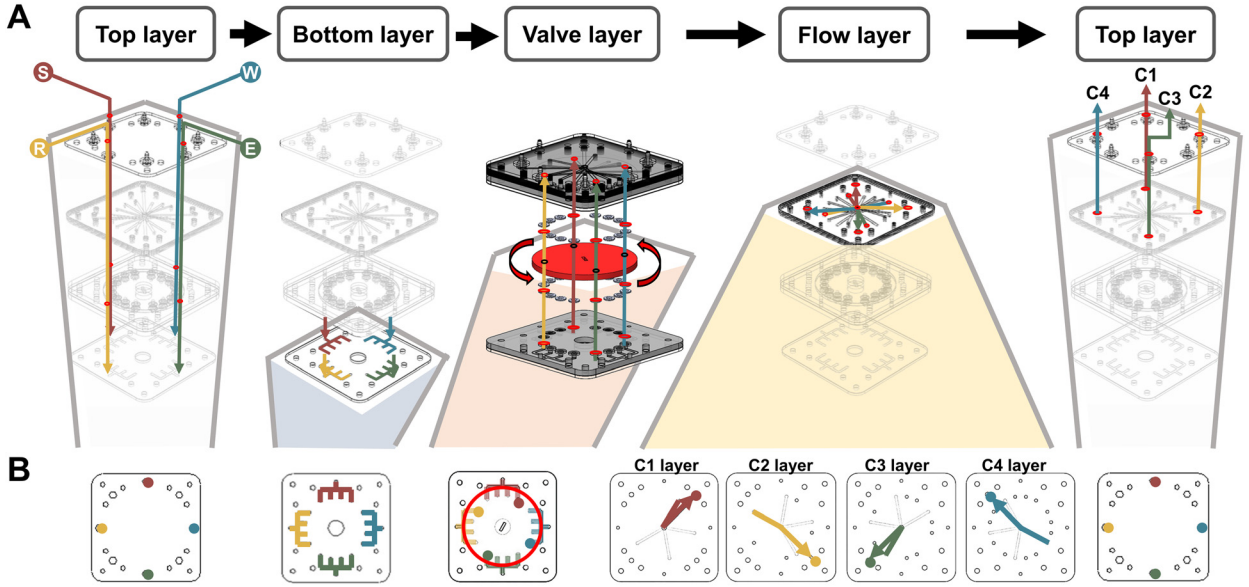

Fig. 2 Programmable flow routing enabled by the ICV. (A) Exploded schematic illustrating the internal structure and fluidic routing logic of the ICV. During operation, fluids from external buffer reservoirs enter the top layer, descend vertically through the valve's central axis, and are sequentially directed through the bottom layer and rotational valve layer. The fluids then traverse the flow layer and return to the top layer *via* designated outlet ports, enabling integration with downstream purification modules. Only the rotary disc in the valve layer rotates; all inlet/outlet ports and microchannel layers remain stationary. Flow paths are color-coded for clarity: sample (S, red), wash (W, cyan), elution (E, green), and re-equilibration (R, yellow). (B) Corresponding top-view schematics of each functional layer. The flow layer is subdivided into four radial zones (C1–C4), each responsible for directing specific buffers to one of four affinity chromatography columns. When activated, incoming liquids are flowed through designated microchannels whose accessibility is governed by the angular position of through-holes on the rotating valve layer. This multilayered configuration enables programmable, column-specific buffer delivery, supporting staggered and parallel purification cycles. The orthogonal arrangement of inlet and outlet paths minimizes dead volume and cross-contamination while ensuring precise spatial and temporal control over fluid routing. The current configuration depicts operation mode I1, in which a designated buffer is routed to column 1 (C1) while the other channels remain closed. This mode is one of four programmed states comprising the complete purification cycle (see Fig. S4 for the full I1–I4 cycle).

actuation (Fig. S3). The bottom layer of the ICV features a palm-like design, with four "finger" channels independently routing the processed liquid upward into each of the four affinity chromatography columns. This architecture supports column-level synchronization, enabling staggered purification cycles in a space-efficient footprint.

The CCV follows a similar structural blueprint but is tailored for real-time collection decision-making. Instead of distributing fluids to multiple output lines, the CCV bifurcates the eluate stream into either the product reservoir or waste outlet (Fig. S2C and D). Its rotational disc dynamically selects which path is open based on real-time feedback from the programmed collection window. This targeted fractionation strategy enables selective retrieval of high-concentration eluates while diverting early/late-phase or dilute fractions to waste, thus enhancing product purity without post-processing.

To ensure the valving mechanism, the stepper motor is mounted beneath the valve module and mechanically coupled to the embedded rotary disc (the red-circled component within the valve layer in Fig. 2A) *via* a coaxial shaft/coupler, allowing the disc to rotate while the surrounding microchannel layers remain stationary. Valving is therefore achieved purely through relative angular alignment: the circumferential through-holes on the disc serve as vertical fluidic vias that either align with the corresponding upstream and downstream ports to establish an "open" connection, or misalign to interrupt the vertical pathway and create a "closed" state. Importantly, only the rotary disc rotates; all distribution and routing microchannels remain fixed in the top/flow/bottom layers, rendering each valve state deterministic and repeatable once a reference (home) angle is defined. These discrete valve states are addressed by commanding the stepper motor to predefined angular positions specified in a PC-controlled operation table executed through the motor driver/controller.

Together, the ICV and CCV form a closed-loop, programmable flow control system that enables the coordinated execution of multi-step purification protocols with precise temporal resolution. By embedding valve logic directly into hardware and decoupling buffer switching from manual operation, the system facilitates continuous protein purification while minimizing dead volume and cross-contamination. To ensure robust performance during repeated operation, the valves were evaluated under various programmed modes for flow-switching accuracy, sealing integrity, and actuation timing. This modular and automation-friendly design provides a foundation for scalable downstream bioprocessing, particularly in applications requiring compactness, reproducibility, and reduced operator intervention.

Programmable operation modes of the ICV and CCV

To enable continuous and synchronized multicolumn purification, the ICV was programmed to operate in four sequential modes (I1–I4), each corresponding to a specific stage of the purification cycle for one chromatography column. In this stepper motor-controlled MCPP platform, these discrete valve modes enable staggered, parallel column operation and thereby sustain uninterrupted

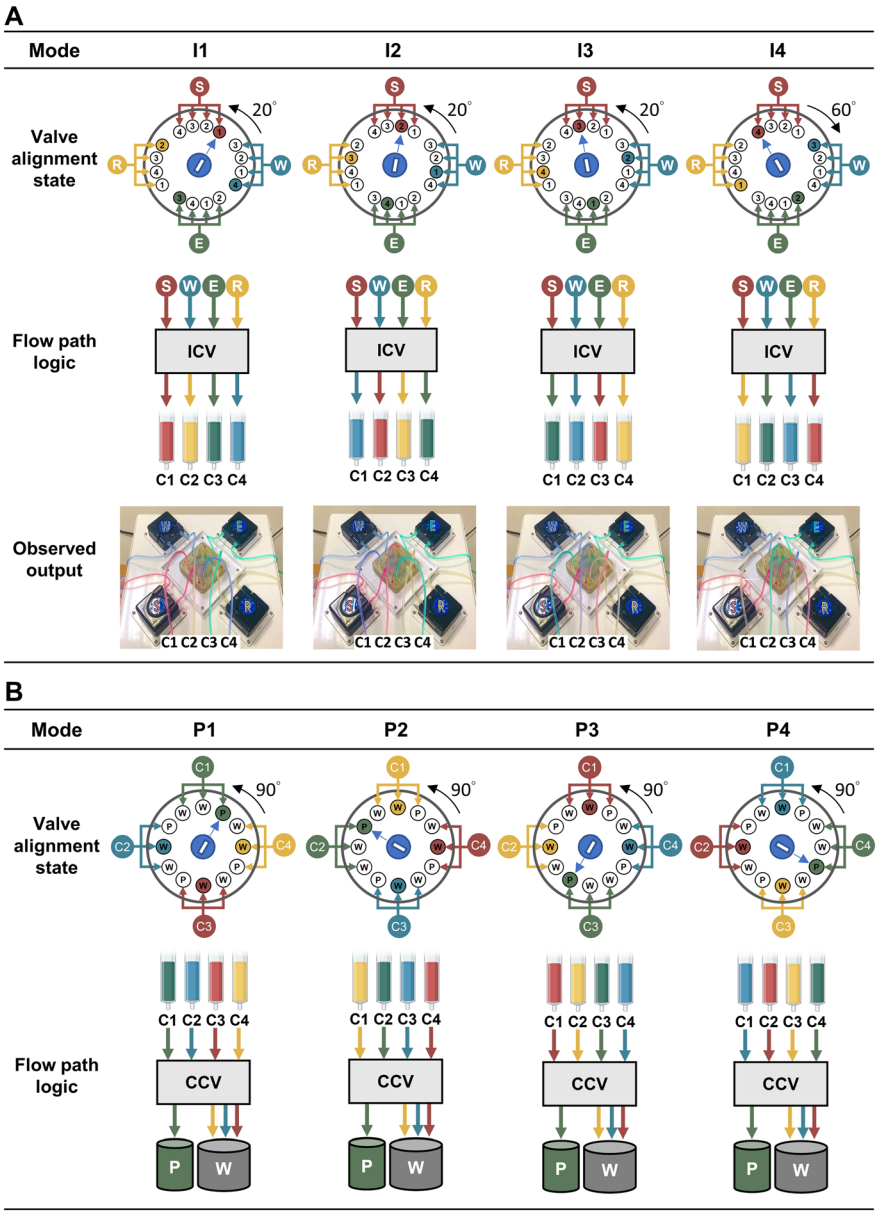

Fig. 3 Programmable operation modes enabled by rotary valve configurations in the ICV and CCV. (A) The ICV operates under four programmable valve alignment states (I1–I4), each defining a distinct rotary valve configuration that directs one of four buffer solutions: sample (S), wash (W), elution (E), or re-equilibration (R) to a specific chromatography column (C1–C4). This staggered assignment enables synchronized, parallel purification cycles across columns in a continuous workflow. The valve alignment state (top panel) visualizes the rotary-disc position at each programmed angle; highlighted color-coded connections indicate OPEN vertical pathways formed when a disc through-hole simultaneously aligns with the corresponding stationary inlet port (S/W/E/R) and outlet port (C1–C4), whereas non-highlighted connections are CLOSED. An arrow at the disc center indicates the disc orientation for each mode (I1–I4) using the sample (S) position as a visual reference; it denotes rotational indexing rather than flow direction, while the remaining buffer connections (W/E/R) are fully specified by the color-coded open/closed linkages. Red-numbered through-holes denote OPEN (aligned) states, whereas blank positions are CLOSED (misaligned). The middle panel illustrates the programmed flow path logic based on valve alignment, and the bottom panel shows corresponding experimental validation using color-coded dyes that were selectively routed to each column under the respective modes. (B) The CCV similarly rotates through four product collection modes (P1–P4), each determining the outlet routing configuration. In each mode, eluates from a designated active column are directed to the product reservoir (P), while outputs from the remaining columns are diverted to the waste reservoir (W). The valve alignment state and flow path logic are interpreted using the same open/closed definition as in (A), enabling angle-addressable, time-gated fraction collection for real-time purification decisions.

cycling across all columns. In each mode, the ICV directs one of the four buffer types—sample (S), wash (W), elution (E), or re-equilibration (R)—into a designated column, while the remaining three buffers are routed to the other columns in the cycle (Fig. 3A). The valve alignment state visualizes the rotary-disc position at each programmed angle and indicates which stationary inlet port (S/W/E/R) is fluidically connected to which stationary outlet port (C1–C4). In each mode, the highlighted color-coded connections indicate an OPEN vertical pathway formed when a through-hole on the rotating disc simultaneously aligns with the corresponding upstream (flow/distribution layer) and downstream (bottom routing layer) ports, whereas non-highlighted ports are CLOSED. The flow path logic summarizes the same connectivity as a simplified routing diagram, and the bottom row provides experimental verification using color-coded dyes delivered to the four columns. For example, in mode I1, the sample buffer is delivered to column C1, while wash, elution, and re-equilibration buffers are routed to C2, C3, and C4, respectively (Fig. S4 and Movie S1).

Mode transitions are implemented by fixed rotational increments of the valve disc. Progression from mode I1 to I4 occurs through successive 20° counterclockwise rotations. Upon completion of I4, the disc returns to I1 *via* a 60° clockwise rotation to complete one full operational cycle. Correspondingly, the angular positions follow the sequence 30°, 10°, 350°, 330°, and 30°. This rotation scheme encodes the buffer–column pairing while maintaining continuous, staggered cycling without downtime. As the I1–I4 sequence repeats, each column sequentially undergoes sample loading, washing, elution, and re-equilibration in a staggered manner; upon returning to I1, the cycle resumes without interruption, thereby sustaining continuous multicolumn purification while ensuring identical processing stages across columns.

The CCV follows a complementary mode-switching logic to manage real-time product collection. During active collection, the CCV rotates through four product modes (P1–P4), each aligning the flow path to selectively direct eluates from one of the four columns to the product reservoir (P), while diverting outputs from the remaining three columns to waste (W) (Fig. 3B and S5). In the valve alignment state for the CCV, the highlighted connections indicate which column effluent is actively routed to P at the current programmed angle, while the remaining effluents are directed to W. These modes are executed *via* 90° counterclockwise steps, rotating from 30° to 300°, 210°, and 120° before returning to the original 30° position in a final 90° step, thereby completing one full collection cycle. Once the concentration of the target protein in the active column drops below a predefined threshold, the CCV transitions to the corresponding waste mode (W1–W4), in which all eluates are routed to waste (Fig. S6), minimizing dilution of the product stream and reducing background contamination.

This dynamic valve coordination between the ICV and CCV ensures fully automated column cycling and high-resolution fraction selection. By encoding stage-specific flow paths into discrete valve angles, the system achieves programmable, real-time control of multistep purification with minimal cross-talk, reduced dead volume, and no manual intervention, establishing a robust foundation for scalable, continuous downstream bioprocessing.

Time-resolved fraction collection improves product purity *via* programmable MCPP control

The operational stability and purification performance of the ICV were assessed in a 10-cycle continuous run using a model crude lysate containing a 1 : 1 mixture of GFP-His_6 and red fluorescent protein (RFP). GFP-His_6 served as the affinity-binding target, whereas RFP acted as a non-binding impurity for visual and quantitative tracking. As shown in Fig. 4A, the ICV selectively routed distinct buffers to individual columns according to a programmed operation table that defined buffer identity, flow rate, and timing for each purification stage (Fig. 4B). Each 32 min cycle included four automated steps—sample loading, washing, elution, and re-equilibration—executed without manual intervention or system reset. A high-flow rinse during washing efficiently removed loosely bound proteins, followed by a brief static pause during elution to facilitate imidazole equilibration and target release from the Ni-NTA resin.

Under UV illumination, eluates exhibited intense green fluorescence from GFP, while waste fractions retained the red fluorescence signal from RFP (Fig. 4C). SDS-PAGE confirmed consistent recovery of the target protein as a ~28 kDa band across all 10 cycles (Fig. 4D). Quantitative analysis by Bradford assay and densitometry indicated product purity ranging from 70% to 88% (Fig. 4E). These results demonstrate that the ICV enables stable, reproducible, and fully automated multi-step purification over extended operation, validating its role as the upstream module in a scalable, continuous-flow protein purification platform.

Time-resolved fraction collection improves product purity *via* programmable MCPP control

To implement real-time fraction selection and enhance product purity, the control strategy was expanded to coordinate both the ICV for multi-column operation and the CCV for automated, time-resolved fraction collection (Fig. 5A). In this configuration, the complete MCPP was applied to purify GFP-His_6 from a crude lysate containing RFP and other bacterial proteins. The objectives were to (i) define the optimal elution window for target recovery and (ii) validate the CCV's capability to selectively direct high-concentration fractions based on elution timing. A two-cycle automated purification run was performed, with each 32 min cycle comprising sample loading, washing, elution, and re-equilibration as defined by the programmed operation table (Fig. 5B). During the elution phase, fractions were manually collected at 30 s intervals and analyzed by SDS-PAGE and Bradford assay to quantify protein concentration and purity (Fig. 5C). The elution profile revealed that the majority of GFP-His_6 was recovered within the first 3 min, corresponding to the highest-purity fractions.

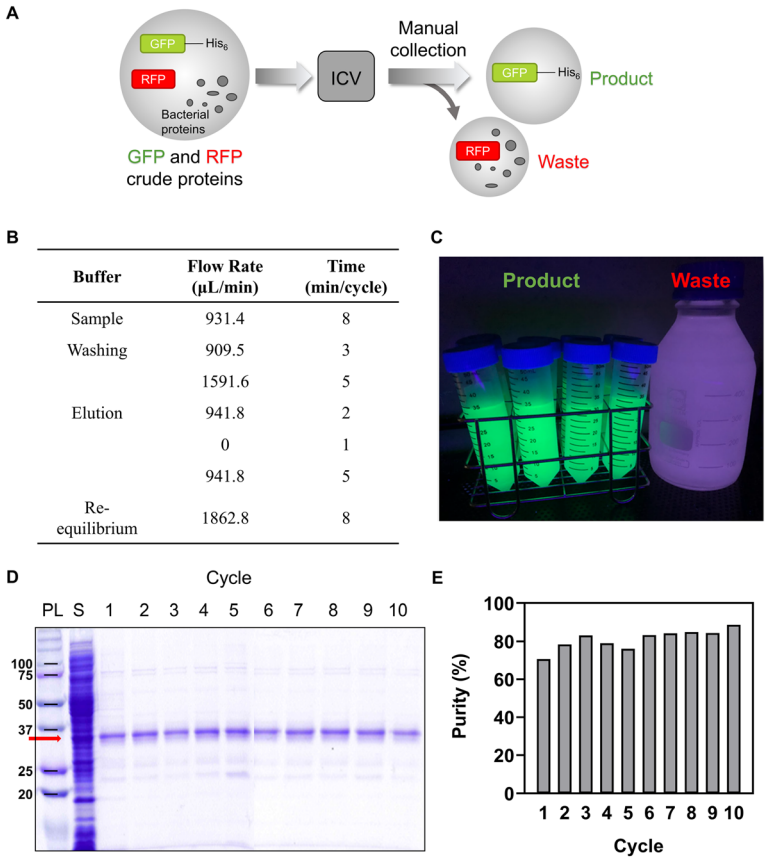

Buffer	Flow Rate (μL/min)	Time (min/cycle)
Sample	931.4	8
Washing	909.5	3
	1591.6	5
Elution	941.8	2
	0	1
	941.8	5
Re-equilibrium	1862.8	8

Fig. 4 Continuous purification of GFP-His_6 using the ICV module. (A) Schematic of the ICV-based separation workflow. A 1 : 1 crude protein mixture of His_6-tagged GFP (target) and RFP (non-binding impurity) was processed through the ICV, where GFP was captured on Ni-NTA resin and eluted to the product reservoir, while RFP and other bacterial proteins were directed to waste. (B) Programmed operation table specifying buffer type, flow rate, and duration for each stage of the 32 min purification cycle (sample loading, washing, elution, and re-equilibration), executed autonomously by the ICV without manual intervention. (C) UV fluorescence images of collected fractions, showing bright green fluorescence in GFP-containing eluates and red-purple fluorescence from RFP in waste fractions, confirming selective separation. (D) SDS-PAGE of eluates from 10 consecutive purification cycles, showing a consistent ~28 kDa band (red arrow) corresponding to GFP-His_6. PL: protein ladder; S: crude sample. (E) Purity quantification by Bradford assay and densitometric analysis, showing stable values between 70% and 88% across all 10 cycles, demonstrating the ICV's robustness for sustained, automated operation under continuous-flow conditions.

Using these data, the operation table was refined to program the CCV for selective collection. During the defined 3 min high-concentration window, eluates from each column (P1–P4) were directed into the product reservoir; outside this window, the CCV switched to waste outlets (W1–W4) to discard late-stage, lower-purity fractions. A real-time demonstration of the complete MCPP is provided in Movie S2, showing continuous GFP collection through the CCV under 4 °C operation, corroborating synchronized ICV/CCV control and uninterrupted, contamination-free product recovery. SDS-PAGE confirmed successful enrichment of GFP-His_6 from all four columns across both purification cycles (Fig. 5E), with purity consistently maintained between 80% and 85% (Fig. 5F).

These results demonstrate that integrating synchronized delivery and collection valve control enables time-resolved fraction selection, effectively minimizing dilution from tailing fractions while reducing downstream processing requirements. This approach underscores the versatility of the MCPP for fully automated, high-purity protein purification.

Functional validation of purified therapeutic protein

To evaluate the ability of the MCPP to preserve the functional integrity of a clinically relevant therapeutic protein, His_6-tagged human TRAIL (hTRAIL; ~23 kDa) was selected as a model target. hTRAIL is a pro-apoptotic cytokine that selectively induces apoptosis in tumor cells while sparing normal tissues, making it a promising candidate for targeted cancer therapy.[21] Purification was performed using the same fully automated schedule and valve control logic established for GFP-His_6. During the elution phase, fractions were collected at 30 s intervals and analyzed *via* Bradford assay and SDS-PAGE. Consistent with previous experiments, hTRAIL was predominantly recovered within the first 2–3 min of elution, with early fractions achieving 80–89% purity (Fig. 6A).

To assess biological activity, dialyzed hTRAIL fractions were applied to A549 human lung carcinoma cells, a well-established model for evaluating TRAIL-induced apoptosis. After 24 h of incubation, cell viability decreased in a concentration-dependent manner, yielding an IC_{50} of approximately 125 ng

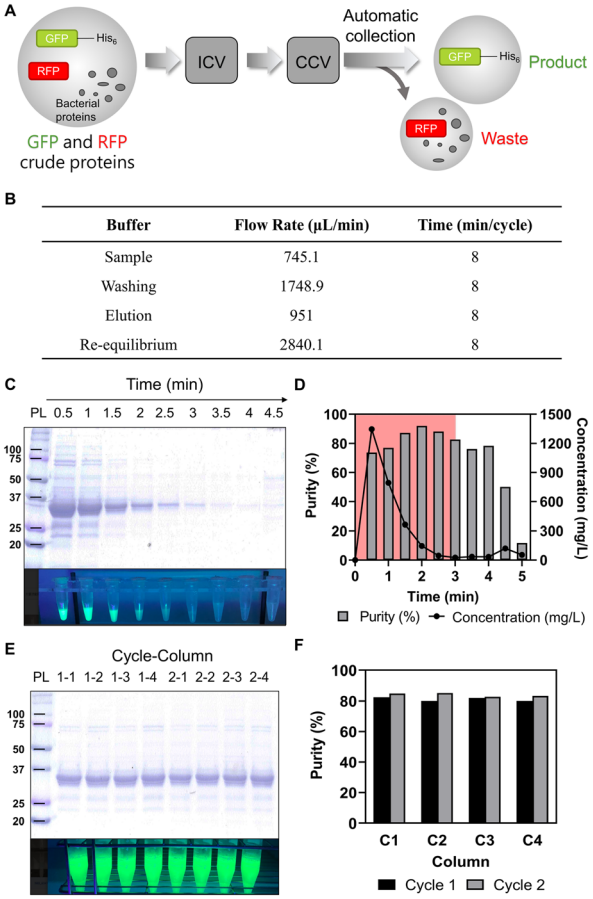

Buffer	Flow Rate (μL/min)	Time (min/cycle)
Sample	745.1	8
Washing	1748.9	8
Elution	951	8
Re-equilibrium	2840.1	8

Fig. 5 Time-resolved fraction selection using the complete MCPP platform. (A) Schematic of the MCPP integrating the ICV for multi-column coordination and the CCV for automated, time-based fraction collection. A crude lysate containing His_6-tagged GFP (target) and RFP with other bacterial proteins (non-binding impurities) was processed through the MCPP, where GFP was selectively captured, eluted, and directed to the product reservoir, while impurities were diverted to waste. (B) Programmed operation table specifying buffer type, flow rate, and step duration for each stage of the 32 min purification cycle. (C) SDS-PAGE of eluates collected every 30 s during the elution phase (upper panel), paired with UV fluorescence images (lower panel) showing GFP distribution. (D) Elution profile from (C), with protein concentration (solid line) and purity (bars) over time. The first 3 min (pink region) yielded peak GFP concentration and were defined as the programmed product collection window for the CCV. (E) SDS-PAGE (upper panel) and fluorescence images (lower panel) of fractions selectively collected during the high-yield window across four columns over two purification cycles. (F) Quantification of GFP purity from (E), showing consistent values of 80–85% across all columns and both cycles.

mL^{-1} (Fig. 6B). This value falls within the reported activity range for recombinant hTRAIL, confirming that the MCPP process preserved both the structural integrity and bioactivity of the protein.

These findings demonstrate that the MCPP platform can deliver high-purity therapeutic proteins while maintaining their functional properties—an essential requirement for clinical translation and biopharmaceutical manufacturing where therapeutic efficacy is activity-dependent.

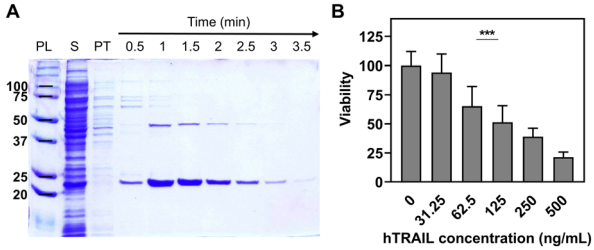

Fig. 6 Functional validation of purified His_6-tagged hTRAIL. (A) SDS-PAGE of hTRAIL eluates (MW ~ 23 kDa) collected every 30 s during the elution phase, showing that high-purity protein (80–89%) was recovered predominantly within the first 2–3 min. (B) Viability of A549 human lung carcinoma cells after 24 h treatment with increasing concentrations of purified hTRAIL. A significant, dose-dependent decrease in viability was observed, with an IC_{50} of ~125 ng mL^{-1} (***$p < 0.001$, $n = 3$), confirming that the MCPP process preserved the protein's biological activity post-purification.

Discussion

We have developed a digitally programmable, fully automated MCPP platform that integrates microfluidic inlet and collection valves for continuous, high-fidelity separation. The time-rotating ICV enables synchronized buffer exchange and column cycling, while the CCV allows real-time, concentration-based fraction selection. Together, these modules form a closed-loop, logic-driven system capable of executing multi-step chromatography workflows with precise temporal control. The platform's stability and performance were validated in a 6-hour, 10-cycle continuous run, where His_6-tagged GFP was consistently recovered at >70% purity across four parallel columns. By selectively collecting only the high-concentration fraction during elution, the CCV increased product purity to 80–89% while minimizing dilution from late-stage eluates. This gating strategy reduces dependence on downstream polishing and represents a meaningful advancement in dynamic fraction control for protein purification. To demonstrate applicability in therapeutic protein production, we purified His_6-tagged hTRAIL, a pro-apoptotic cytokine with high clinical relevance. Post-purification assays confirmed dose-dependent cytotoxicity against A549 carcinoma cells, with an IC_{50} of ~125 ng mL^{-1}, indicating that the purification process preserved both structural integrity and biological function. This finding underscores the system's suitability for labile or activity-dependent biopharmaceuticals.

In the broader context of downstream bioprocessing, it is useful to benchmark the MCPP method against performance ranges reported for conventional laboratory-scale affinity chromatography. Vendor protocols for 1 mL His-tag columns typically recommend ~5 column volumes (CV) for equilibration, 10–15 CV for washing, and ~5 CV for elution at around 1 CV min^{-1}, which already corresponds to 20–25 min of chromatography time per run, excluding sample loading and re-equilibration. Spin- and FPLC-based protein A/G kits similarly report complete one-step purification within roughly 20–60 min, depending on column format and scale.[22] In this context,

the MCPP completes a full multi-step cycle in ~8–10 min at sub-milliliter volumes, offering a several-fold reduction in processing time and buffer consumption while preserving chromatographic resolution. In most batch or FPLC workflows, fraction collection windows are still defined by UV chromatogram interpretation and operator- or script-defined timing, rather than hard-wired, state-based logic at the fluidic level.[23] In contrast, the CCV module in the MCPP deterministically gates eluate based on pre-defined temporal windows, achieving sub-minute boundary discrimination without external detectors or manual adjustment.

In continuous, multi-step protein purification on microfluidic platforms, robust valves are crucial for coordinating buffer exchange (sample loading/washing/elution/reequilibration), column circulation, and fraction selection while minimizing dead volume. Past microfluidic purification platforms have employed various valve technologies to achieve these functions, differing in required actuation structures, scalability, and material stability. For instance, pneumatic membrane valve systems offer high integration density and rapid switching through pressure-driven membrane deformation.[24] However, they typically require auxiliary pneumatic components (*e.g.*, pressure sources and multiple control lines), increasing setup complexity when porting workflows between different laboratories. In contrast, electromagnetically and mechanically driven microvalves reduce reliance on pneumatic components and provide deterministic on/off control, but scaling to multiple parallel flow paths may require additional actuators and encapsulation.[25] Rotary multiport valves connect multiple states through a single rotation angle, enabling deterministic switching and routing.[26] For chromatography-oriented applications, these designs still require precise sealing and angular positioning to maintain stable alignment during prolonged, repetitive cycles. Against this backdrop, our proposed stepper motor-driven rotary ICV/CCV architecture offers a compromise between deterministic path planning and modular scalability, suitable for continuous chromatography workflows. Compared to the strategies mentioned above, our method simplifies the control structure by using two dedicated actuators for valving (ICV for upstream buffer path planning and CCV for downstream fraction selection) to achieve programmable switching, eliminating the need for pneumatic devices and multi-line control. Multi-port connections are implemented through predefined angular positions, enabling multi-buffer-to-multi-column path planning and timed fraction collection, and employing a compact drive scheme compatible with chromatographic steps and multi-column cycles. Overall, the MCPP platform provides a compact approach to automated fluid routing and fraction selection for continuous purification workflows, with reduced dead volume and minimized cross-talk.

A key advantage of the platform lies in its modular and disposable polymer-based construction, which supports single-use operation, eliminates cleaning requirements, and mitigates cross-contamination risks. However, the current fixed-concentration elution mode may not be optimal for proteins with variable binding affinities or complex elution kinetics. To address this limitation, we are developing an integrated microfluidic passive mixer to enable continuous gradient elution, which would allow real-time fine-tuning of elution profiles for heterogeneous analytes without adding architectural complexity.

Looking forward, integration of real-time sensor data with predictive models and protein-specific databases could enable adaptive control over elution timing, buffer composition, and collection thresholds, even for unknown targets.[27–29] The incorporation of machine learning algorithms could allow the system to self-optimize based on prior purification outcomes, thereby accelerating method development, improving reproducibility, and reducing resource consumption.[30,31] This capability would be particularly valuable for rapid-response manufacturing scenarios—such as therapeutic protein production during pandemics—where speed, consistency, and product quality are critical. While this study focused on immobilized metal affinity chromatography (IMAC), the platform's fluidic architecture is compatible with additional modes such as ion-exchange and hydrophobic interaction chromatography.[32,33] This flexibility is essential for multi-step workflows, including monoclonal antibody purification, which often requires sequential protein A/G/L capture and tailored polishing steps. The compact form factor and automated control also make the system suitable for decentralized production or point-of-care settings. When integrated with upstream fermentation modules, it could enable end-to-end continuous bioprocessing with minimal production footprint.[34,35]

Conclusions

In summary, we present a compact, digitally programmable protein purification system that combines microfluidic precision, automated control, and single-use architecture to deliver high-purity, functionally active proteins in a continuous manner. Demonstrated across multiple protein targets, the platform addresses persistent challenges in scalability, reproducibility, and contamination control, and provides a foundation for next-generation purification workflows. With future enhancements such as gradient elution, multi-mode chromatography, and AI-driven optimization, this system has the potential to transform both industrial biomanufacturing and personalized therapeutic protein production.

Author contributions

Y. C. L., C. Y. H., and Y. C. T. contributed equally to this work. C. H. W., Y. H. C., and I. W. C. initiated the research; J. H. H. supervised, and conceptualized, and identified authentic messages of the project; C. H. W., Y. H. C., I. W. C., H. Y. M., Y. H. L. Y. C., and F. F. H. designed the experiments; Y. C. L., C. Y. H., and Y. C. T. performed the experiments; Y. C. L., C. Y. H., Y. C. T., and C. H. W. analyzed the data and

drew figures; Y. C. L., C. Y. H., Y. C. T., and J. H. H. wrote, edited, and reviewed the manuscript before submission.

Conflicts of interest

There are no conflicts to declare.

Data availability

The data supporting this article have been included as part of the supplementary information (SI).

Supplementary information: includes operation of the ICV (Movie S1), MCPP system continuous purification (Movie S2), GUI screenshot (Fig. S1), design of the ICV and CCV (Fig. S2), design of the valve layer (Fig. S3), fluid routing in ICV mode (Fig. S4), in CCV product mode (Fig. S5), and in CCV waste mode (Fig. S6). See DOI: https://doi.org/10.1039/d6lc00015k.

Acknowledgements

This work was financially supported by the National Science and Technology Council (NSTC), Taiwan, under grant numbers 107-2221-E-007-041-MY3, 110-2221-E-007-013-MY3, and 110-2628-E-007-002. The authors would like to thank Hsiao-Ching Lin (Academia Sinica) and Claire Roa-Pu Shen (National Tsing Hua University) for their guidance on recombinant protein expression and protein analysis. We are also grateful to Ping-Chiang Lyu (National Tsing Hua University) for his valuable suggestions.

Notes and references

1 G. Walsh and E. Walsh, *Nat. Biotechnol.*, 2022, **40**, 1722–1760.
2 H. Rahalkar, A. Sheppard, C. A. Lopez-Morales, L. Lobo and S. Salek, *Pharm. Med.*, 2021, **35**, 235–251.
3 Y. H. Oh, M. L. Becker, K. M. Mendola, L. H. Choe, L. Min, K. H. Lee, Y. Yigzaw, A. Seay, J. Bill, X. Li, D. J. Roush, S. M. Cramer, S. Menegatti and A. M. Lenhoff, *Biotechnol. Bioeng.*, 2023, **120**, 1068–1080.
4 M. Kesik-Brodacka, *Biotechnol. Appl. Biochem.*, 2018, **65**, 306–322.
5 C. Sánchez-Trasviña, M. Flores-Gatica, D. Enriquez-Ochoa, M. Rito-Palomares and K. Mayolo-Deloisa, *Front. Bioeng. Biotechnol.*, 2021, **9**, 717326.
6 D. Morimoto and E. Walinda, *Protein Expression Purif.*, 2024, **223**, 106560.
7 J. J. Milne, in *Protein Chromatography: Methods and Protocols*, ed. S. T. Loughran and J. J. Milne, Springer US, New York, NY, 2023, pp. 61–75, DOI: 10.1007/978-1-0716-3362-5_5.
8 S. Liu, Z. Li, B. Yu, S. Wang, Y. Shen and H. Cong, *Adv. Colloid Interface Sci.*, 2020, **284**, 102254.
9 J. Steen, M. Uhlén, S. Hober and J. Ottosson, *Protein Expression Purif.*, 2006, **46**, 173–178.
10 H. Li, P. Rose, P. Rowicki, C. Cutler, J. T. McPhee, C. Frey, L. Lemieux, G. Pelette, J. K. Ang, R. Liu and D. D. Richardson, *Biotechnol. Prog.*, 2024, **40**, e3434.
11 A. S. Ransdell, M. Reed, J. Herrington, P. Cain and R. M. Kelly, *Protein Expression Purif.*, 2023, **207**, 106269.
12 A. L. Zydney, *Curr. Opin. Chem. Eng.*, 2015, **10**, 8–13.
13 A. L. Zydney, *Biotechnol. Bioeng.*, 2016, **113**, 465–475.
14 R. Patil and J. Walther, in *New Bioprocessing Strategies: Development and Manufacturing of Recombinant Antibodies and Proteins*, ed. B. Kiss, U. Gottschalk and M. Pohlscheidt, Springer International Publishing, Cham, 2018, pp. 277–322, DOI: 10.1007/10_2016_58.
15 V. Jossen, R. Eibl, G. Broccard and D. Eibl, in *Biopharmaceutical Manufacturing: Progress, Trends and Challenges*, ed. R. Pörtner, Springer International Publishing, Cham, 2023, pp. 3–38, DOI: 10.1007/978-3-031-45669-5_1.
16 Y. Yang, Y. Chen, H. Tang, N. Zong and X. Jiang, *Small Methods*, 2020, **4**, 1900451.
17 Z. Liu, F. Fontana, A. Python, J. T. Hirvonen and H. A. Santos, *Small*, 2020, **16**, 1904673.
18 A. Jungbauer, P. Satzer, A. Duerauer, A. Azevedo, R. Aires-Barros, B. Nilsson, S. Farid, S. Goldrick, M. Ottens, M. Sponchioni and H. Marcelo Fernandez Lahore, *Sep. Purif. Technol.*, 2024, **338**, 126439.
19 V. Sharma, A. Mottafegh, J.-U. Joo, J.-H. Kang, L. Wang and D.-P. Kim, *Lab Chip*, 2024, **24**, 2861–2882.
20 H.-L. Hsieh, P. Nath and J.-H. Huang, *ACS Biomater. Sci. Eng.*, 2019, **5**, 4852–4860.
21 J. H. Stegehuis, L. H. A. M. de Wilt, E. G. E. de Vries, H. J. Groen, S. de Jong and F. A. E. Kruyt, *Drug Resistance Updates*, 2010, **13**, 2–15.
22 Cytiva, *Affinity Chromatography Handbook, Vol. 2: Tagged Proteins*, Cytiva, Uppsala, Sweden, 2021.
23 J. A. Asenjo and B. A. Andrews, *J. Mol. Recognit.*, 2009, **22**, 65–76.
24 J.-Y. Qian, C.-W. Hou, X.-J. Li and Z.-J. Jin, *Micromachines*, 2020, **11**, 172.
25 X. Liu and S. Li, *SLAS Technol.*, 2014, **19**, 444–453.
26 D. R. Miller, D. K. Schaffer, M. D. Neely, E. S. McClain, A. R. Travis, F. E. Block, J. R. McKenzie, E. M. Werner, L. Armstrong, D. A. Markov, A. B. Bowman, K. C. Ess, D. E. Cliffel and J. P. Wikswo, *Sens. Actuators, B*, 2021, **341**, 129972.
27 C. Shi, Z. Y. Gao, Q. L. Zhang, S. J. Yao, N. K. H. Slater and D. Q. Lin, *J. Chromatogr. A*, 2020, **1619**, 460936.
28 A. Pareek, V. S. Buddhiraju, V. S. Masampally, K. Premraj and V. Runkana, *Biotechnol. Prog.*, 2023, **39**, e3376.
29 S. Chan, N. Titchener-Hooker, D. G. Bracewell and E. Sørensen, *AIChE J.*, 2008, **54**, 965–977.
30 N. Saxena, G. Thakur, N. G. Jesubalan, A. Kulkarni, V. Yezhuvath and A. Rathore, *Comput. Chem. Eng.*, 2022, **164**, 107896.
31 D. G. Sauer, M. Melcher, M. Mosor, N. Walch, M. Berkemeyer, T. Scharl-Hirsch, F. Leisch, A. Jungbauer and A. Dürauer, *Biotechnol. Bioeng.*, 2019, **116**, 1999–2009.
32 O. Kökpinar, D. Harkensee, C. Kasper, T. Scheper, R. Zeidler, O. W. Reif and R. Ulber, *Biotechnol. Prog.*, 2006, **22**, 1215–1219.
33 T. N. Lin and S. C. Lin, *J. Biosci. Bioeng.*, 2022, **133**, 258–264.

34 H. Schwarz, J. Gomis-Fons, M. Isaksson, J. Scheffel, N. Andersson, A. Andersson, A. Castan, A. Solbrand, S. Hober, B. Nilsson and V. Chotteau, *Biotechnol. Bioeng.*, 2022, **119**, 2152–2166.

35 V. Chopda, A. Gyorgypal, O. Yang, R. Singh, R. Ramachandran, H. Zhang, G. Tsilomelekis, S. P. S. Chundawat and M. G. Ierapetritou, *J. Chem. Technol. Biotechnol.*, 2022, **97**, 2317–2335.